Inorganic Chemistry

pubs.acs.org/IC

Article

Photosensitizers Based on Bichromophoric Dyads Combining Ru(II)-Polypyridyl Complexes and Dissymmetric Perylene Monoimide Derivatives: The Nontrivial Role of Ligand Substitution

Gina Elena Giacomazzo, Sandra Doria, Andrea Revilla-Cuesta, Nicola De Monte, Marco Pagliai, Giangaetano Pietraperzia, Barbara Valtancoli, Tomás Torroba, Luca Conti,* Mariangela Di Donato,* and Claudia Giorgi

Cite This: https://doi.org/10.1021/acs.inorgchem.3c04569

Read Online

ACCESS | Metrics & More | Article Recommendations | Supporting Information

ABSTRACT: The covalent modification of Ru(II) polypyridyl complexes (RPCs) with organic chromophores is a powerful strategy to obtain metal-based photosensitizer agents (PSs) with improved performance for application in photodynamic therapy (PDT). In this respect, perylene-imides are of particular interest due to their rich chemical−physical repertoire, and it is therefore quite surprising that their combination with RPCs has been poorly considered so far. Herein, we report on the photophysical behavior of two newly synthesized RPCs bearing a perylene monoimide appendant (PMI-Ad). Differently from the majority of RPCs-perylene-imides dyads, these chromophores are dissymmetric and are tethered to the metal centers through a single C−C bond in the 3- or 5-position of 1,10-phenanthroline (**Ru-3PMI-Ad** and **Ru-5PMI-Ad**). Both compounds show excellent singlet oxygen photosensitizing activity, with quantum yields reaching >90% in the case of **Ru-3PMI-Ad**. A combined spectroscopic and theoretical analysis, also involving transient absorption and luminescence lifetime measurements, demonstrates that both compounds undergo intersystem crossing on a very fast time scale (tens of picoseconds) and with high efficiency. Our results further demonstrate that the increased electron delocalization between the metal center and the PMI-Ad chromophore observed for **Ru-3PMI-Ad** additionally contributes to increase the singlet oxygen quantum yields by prolonging the lifetime of the triplet state.

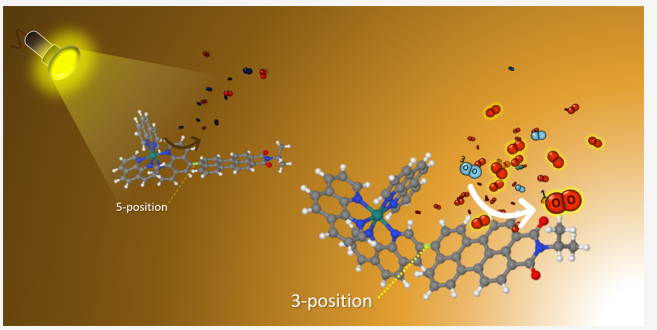

INTRODUCTION

Ruthenium polypyridyl complexes (RPCs) continue to attract increasing interest for their use in photodynamic therapy (PDT), a therapeutic cancer treatment relying on the photoactivation of a photosensitizer molecule, ultimately producing harmful cytotoxic oxygen species. The main advantage of this method as compared with traditional therapies is the complete spatiotemporal control over the drug activation, allowing to considerably limit the side effects normally associated with chemotherapy.[1−4] The interest in employing RPCs as PDT photosensitizers arises from the possibility of accessing a variety of excited-state configurations[5−7] by tuning the nature of ligands in their octahedral geometries, thus modulating their capacity to efficiently sensitize the formation of singlet oxygen ($^1O_2$), which is highly cytotoxic.[8] Since singlet oxygen ($^1\Delta_g$) is produced from the energy transfer between the triplet excited state of the photosensitizer (PS*) and ground-state molecular oxygen ($^3\Sigma_g^-$) through type II pathways, prolonging the triplet excited-state lifetimes represents a suitable strategy to boost the singlet oxygen sensitizing properties. This can be achieved, for example, by inserting π-expansive chelate ligands in Ru(II) scaffolds, as they can change the lowest-lying excited state from ^{3}MLCT to long-lived intraligand[3] IL states[9]: a classic case is the use of the popular benzo[*i*]dipyrido[3,2-*a*:2′,3′-*c*]-phenazine (dppn) ligand/s.[10,11]

Asides from that, another valid alternative is represented by the decoration of metal-coordinated ligands with distinct organic chromophores having their lowest-lying and long-lived triplet state close in energy to the ^{3}MLCT of the metal-based units. In these bichromophoric arrangements, the ^{3}IL states act as excited-state energy reservoirs that prolong the ^{3}MLCT emission, endowing the resulting dyads with improved sensitizing properties, beyond to augment light absorption in the vis/NIR region.[12]

Received: December 24, 2023
Revised: February 23, 2024
Accepted: March 14, 2024

Scheme 1. Synthetic Route Followed for the Preparation of Ruthenium Complexes Ru-5PMI-Ad and Ru-3PMI-Ad

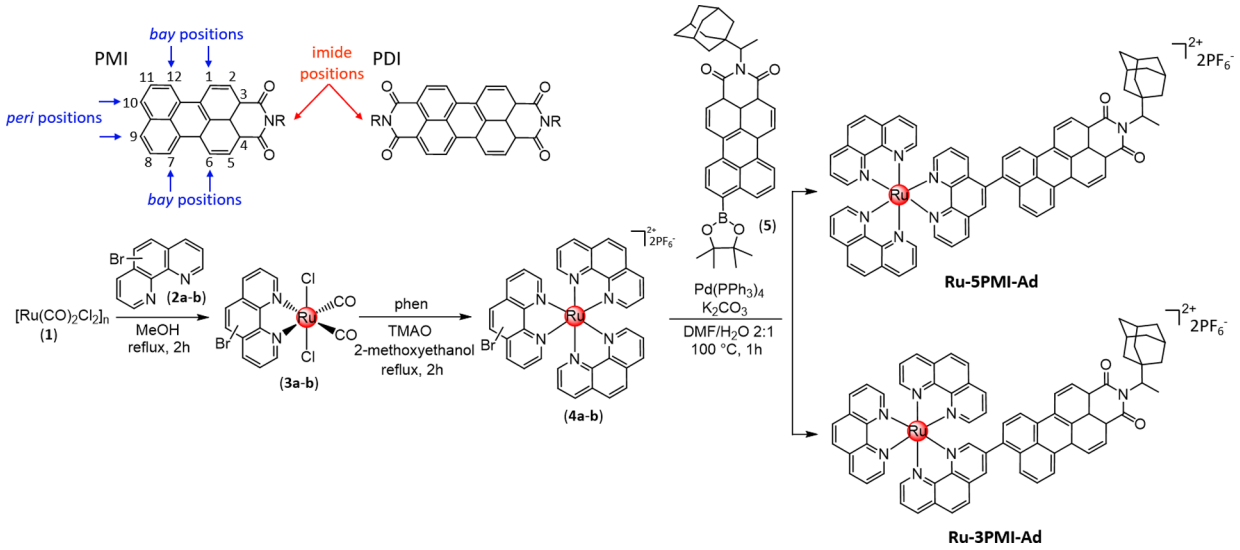

Being first reported by Ford and Rodgers in 1992,[13] this strategy has been used to realize a variety of dyads with improved performances as PSs, where common bidentate chelates of ruthenium, such as bpy (2,2′-bipyridine) or phen (1,10-phenanthroline), were covalently modified with naphthalene-,[14] coumarin-,[15] or pyrene-[16,17] based units. In this context, a great promise arises from the use of perylene-imides, a class of polyaromatic hydrocarbons with extensive π-conjugation that has found application in several areas, spanning from photocatalysis to the design of luminescent probes.[18−20] These molecules are classified into two major classes: perylene diimide (PDI), featuring two electron-withdrawing symmetrical imide moieties on the top and bottom of the electron-rich perylene core, and dissymmetric perylene monoimide (PMI), with only one imide group (Scheme 1). Their multifaceted properties, such as high thermal and photochemical stability, high molar absorptivity, remarkable photoluminescence, and impressive electron-accepting properties, make them ideal candidates as novel RPC-based PSs. It is therefore quite surprising that, so far, RPCs bearing perylene imide derivatives have mostly been applied in photocatalysis and electron transfer,[21−28] whereas only a couple of examples highlighted their potential for PDT.[29,30] Moreover and importantly, the majority of these systems feature symmetric PDI chromophores, conjugated in the bay or imide positions: far fewer systems containing PMI were instead described,[30,31] likely due to their more complex synthetic routes.

This scenario prompted us to investigate the photophysical properties of **Ru-5PMI-Ad** and **Ru-3PMI-Ad**, two newly synthesized RPCs where a phen ligand of a classical $Ru(phen)_3$-core was functionalized at positions 5 or 3 with a PMI derivative (PMI-Ad); this was in turn gathered with a bulky aliphatic group (1-adamantyl-ethylamine, Ad) to overcome inherent aggregation and solubility issues (Scheme 1). In general, a key role in bichromophoric systems is played by the linker (or spacer) between the appended residues and metal-based subunits, as its different features (i.e., length and partial/full conjugation) influence the attitude of the whole system to maintain (or not) the individual properties of the distinct subunits. Contrary to the great majority of already reported perylene-RPCs, where chromophores are tethered to Ru(II)-chelates through their imido nitrogens, causing electronic decoupling with the metal cores,[30,32] in our case the PMI-Ad moieties are directly conjugated to the phen units via a C−C bond, thus endowing the corresponding RPCs of augmented electronic coupling between their subunits. The two different positions for the PMI-Ad substitution in Scheme 1 were considered to investigate their influence on the photophysical properties of the resulting dyads.

EXPERIMENTAL SECTION

Materials. All materials were of reagent grade and used without further purification unless otherwise specified. 5-Bromo-1,10-phenanthroline (**2a**) and 3-bromo-1,10-phenanthroline (**2b**) were purchased from Sigma-Aldrich and used without further purification. Intermediates *trans*(Cl)-[Ru(5-bromo-1,10-phen)$Cl_2(CO)_2$] (**3a**) and *trans*(Cl)-[Ru(3-bromo-1,10-phen)$Cl_2(CO)_2$] (**3b**) were prepared by employing a similar procedure to those reported in literature for analogue compounds.[33] The PMI-pinacol boronic ester *N*-(1-(1-adamantyl)ethyl)-8-pinacolylboronateperylene-3,4-dicarboxylmonoimide (**5**) was obtained by Miyaura borylation reaction on the bromine precursor *N*-(1-(1-adamantyl)ethyl)perylene-8-bromo-3,4-dicarboxylmonoimide through a synthetic procedure previously described.[34]

Synthesis of the Intermediate *trans*(Cl)-[Ru(5-Bromo-1,10-phen)$Cl_2(CO)_2$] (3a). The polymeric precursor $[Ru(CO)_2Cl_2]_n$ (**1**) (59 mg, 0.25 mmol) was dissolved in dry methanol under a N_2 atmosphere. Then, 5-bromo-1,10-phenantroline (60 mg, 0.23 mmol) was added, and the reaction mixture was stirred at reflux for 1 h. The white precipitate formed was then filtered off, washed with hot methanol, and dried under vacuum to obtain complex **3a** as a yellow solid.

Yield 46%. ^{1}H NMR (400 MHz, $(CD_3)_2SO$): δ 9.77 (d, J = 4.8 Hz, 1H, **H2**), 9.70 (d, J = 5.2 Hz, 1H, **H9**), 9.10 (d, J = 8.4 Hz, 1H, **H4**), 8.98 (d, J = 8.0 Hz, 1H, **H7**), 8.89 (s, 1H, **H6**), 8.32 (dd, J_1 = 4.0 Hz, J_2 = 8.0 Hz, 1H, **H3**), 8.23 (dd, J_1 = 4.0 Hz, J_2 = 8.0 Hz, 1H, **H8**) ppm. ^{13}C NMR (100 MHz, $(CD_3)_2SO$): δ 197.2, 155.6, 155.3, 146.4, 145.4, 140.1, 132.1, 131.4, 130.4, 128.8, 128.4, 122.0 ppm. IR ν(CO): 2066, 2007 cm^{-1}.

Synthesis of the Intermediate *trans*(Cl)-[Ru(3-Bromo-1,10-phen)$Cl_2(CO)_2$] (3b). Analogously to the synthesis of the intermediate **3a**, the polymeric precursor **1** (117 mg, 0.50 mmol) was dissolved in dry methanol under a N_2 atmosphere and added with 3-bromo-1,10-phenantroline (118 mg, 0.45 mmol). Then, the reaction mixture was heated at reflux, and after 2 h, an orange/yellow powder appeared. The precipitate was filtered off, washed with

https://doi.org/10.1021/acs.inorgchem.3c04569
Inorg. Chem. XXXX, XXX, XXX−XXX

hot methanol, and dried under a vacuum to give complex **3b** as an orange/yellow solid.

Yield 80%. ^{1}H NMR (400 MHz, $(CD_3)_2SO$): δ 9.78 (d, J = 1.2 Hz, 1H, **H2**), 9.68 (d, J = 4.8 Hz, 1H, **H9**), 9.41 (d, J = 1.2 Hz, 1H, **H4**), 9.04 (d, J = 8.4 Hz, 1H, **H7**), 8.44 (d, J = 8.8 Hz, 1H, **H5** or **H6**), 8.32 (d, J = 8.8 Hz, 1H, **H5** or **H6**), 8.22 (dd, J_1 = 4.8 Hz, J_2 = 8.4 Hz, 1H, **H8**) ppm. ^{13}C NMR (100 MHz, $(CD_3)_2SO$): δ 199.7, 195.7, 154.5, 154.0, 144.9, 143.9, 142.2, 140.3, 131.4, 131.0, 129.5, 127.5, 121.0 ppm. IR v(CO): 2063 and 1990 cm^{-1}.

Synthesis of [Ru(phen)$_2$(5-Bromo-1,10-phen)]2PF$_6$ (4a). To a solution of **3a** (50 mg, 0.10 mmol) in 5 mL of degassed 2-methoxyethanol were added 1,10-phenanthroline (37 mg, 0.20 mmol) and trimethylamine *N*-oxide (56 mg, 0.50 mmol). The reaction mixture was stirred for 1 h at reflux under a N_2 atmosphere. After cooling at r.t., the addition of a 0.1 M aqueous solution of KPF_6 (2 mL) allowed the precipitation of complex **4a** as a dihexafluorophosphate salt. After filtration under vacuum, the solid was washed with water and diethyl ether, affording complex **4a** with a high grade of purity to be used in the subsequent synthetic step.

Yield 82%. ^{1}H NMR (400 MHz, $(CD_3)_2CO$): δ 8.91 (d, J = 8.0 Hz, 1H), 8.85 (s, 1H), 8.83−8.75 (m, 4H), 8.77 (d, J = 8 Hz, 1H), 8.51 (d, 1H), 8.49−8.38 (m, 9H), 7.94 (dd, J_1 = 8.0 Hz, J_2 = 12.0 Hz, 1H), 7.88−7.79 (m, 5H) ppm. ^{13}C NMR (100 MHz, $(CD_3)_2CO$): δ 154.6, 154.3, 154.0, 153.7, 149.4, 148.6, 148.5, 137.7, 137.0, 136.7, 131.9, 131.7, 131.6, 131.0, 128.8, 128.7, 127.6, 127.4, 126.8, 126.7, 126.6, 122.2 ppm. HR-MS: calcd for $C_{36}H_{23}N_6BrRu$ $[M]^{2+}$ 361.00997, found $[M]^{2+}$ 361.00901.

Synthesis of [Ru(phen)$_2$(3-Bromo-1,10-phen)]2PF$_6$ (4b). To a solution of **3b** (65 mg, 0.13 mmol) in 7 mL of degassed 2-methoxyethanol were added 1,10-phenantroline (48 mg, 0.26 mmol) and trimethylamine *N*-oxide (74 mg, 0.67 mmol). The reaction mixture was stirred 2 h at reflux under N_2 atmosphere. After cooling at r.t., the addition of 0.1 M aqueous KPF_6 (2 mL) allowed the precipitation of complex **4b** as a dihexafluorophosphate salt, which was collected by filtration under vacuum and washed with water and diethyl ether. **4b** was obtained with a high grade of purity to be used in the next synthetic step.

Yield 75%. ^{1}H NMR (400 MHz, $(CD_3)_2CO$): δ 9.07 (d, J = 2.0 Hz, 1H), 8.85−8.79 (m, 6H), 8.61 (d, J = 4.0 Hz, 1H), 8.52 (d, J = 1.6 Hz, 1H) 8.49 (d, J = 12 Hz, 1H) 8.45−8.37 (m, 6H), 8.33 (d, J = 4.0 Hz, 1H), 7.86−7.79 (m, 6H) ppm. ^{13}C NMR (100 MHz, $(CD_3)_2CO$): δ 154.4, 154.2, 154.16, 153.94, 153.90, 153.7, 153.6, 148.8, 148.7, 148.69, 148.58, 148.55, 148.52, 147.51, 139.5, 137.7, 137.7, 137.6, 132.12, 131.9, 131.8, 131.7, 130.0, 128.8, 128.8, 128.8, 128.8, 127.9, 127.1, 126.9, 126.84, 126.82, 126.8, 126.3, 121.2 ppm. HR-MS: calcd for $C_{36}H_{23}N_6BrRu$ $[M]^{2+}$ 361.00997, found $[M]^{2+}$ 361.00896.

Synthesis of [Ru(phen)$_2$(5-PMI-Ad)]2PF$_6$ (Ru-5PMI-Ad). In a Schlenk apparatus, a solid mixture of complex **4a** (80 mg, 0.08 mmol) and compound **5** (53 mg, 0.09 mmol) was solubilized in 4 mL of a deaerated mixture of dimethylformamide/water 2:1 (v/v). Potassium carbonate (55 mg, 0.40 mmol) was added, and three vacuum/nitrogen cycles were performed. Then, a catalytic amount (1% w/w) of tetrakis(triphenylphosphine)palladium(0) as catalyst was added and three vacuum/nitrogen cycles were performed again. The reaction mixture was stirred at 100 °C for 3 h and then cooled at r.t. and filtered on a Celite pad with methanol to remove the catalyst. The filtered solution was evaporated to dryness and the resulting red solid was solubilized in dichloromethane (60 mL), washed three times with 10 mL of water and once with 10 mL of brine. The organic phase was dried with Na_2SO_4, filtered, and evaporated to dryness. The red crude product was purified via flash chromatography on silica gel (DCM:MeOH 60:1 v/v) to obtain complex **Ru-5PMI-Ad** as a red-orange solid.

Yield 64%. ^{1}H NMR (400 MHz, $(CD_3)_2CO$): δ 8.98−8.80 (m, 6H), 8.78−8.44 (m, 16H), 8.26−8.20 (m, 1H), 7.98−7.82 (m, 6H), 7.76−7.57 (m, 2H), 7.52−7.45 (m, 1H) 5.15−5.08 (m, 1H), 1.98−1.85 (m, 6H), 1.77−1.58 (m, 12H) ppm. ^{13}C NMR (100 MHz, $(CD_3)_2CO$) shown in Figure S24. HR-MS: calcd for $C_{70}H_{51}N_7O_2Ru$ $[M]^{2+}$ 561.65779, found $[M]^{2+}$ 561.65710.

Synthesis of [Ru(phen)$_2$(3-PMI-Ad)]2PF$_6$ (Ru-3PMI-Ad). Analogously to **Ru-5PMI-Ad**, complex **4b** (80 mg, 0.08 mmol) and compound **5** (53 mg, 0.09 mmol) were solubilized in 4 mL of deaerated dimethylformamide/water 2:1 (v/v) in a Schlenk apparatus. Following addition of potassium carbonate (55 mg, 0.40 mmol), three vacuum/nitrogen cycles were performed. Then, a catalytic amount (1% w/w) of tetrakis(triphenylphosphine)palladium(0) was added, and three vacuum/nitrogen cycles were carried out. The reaction mixture was stirred at 100 °C for 3 h, then cooled at r.t. and filtered on a Celite pad with methanol to remove the catalyst. The filtered solution was evaporated to dryness, and the resulting red solid was solubilized in dichloromethane (60 mL) and washed three times with 10 mL of water and once with 10 mL of brine. The organic phase was dried with Na_2SO_4, filtered, and evaporated to dryness. The red crude product was purified via flash chromatography on silica gel (DCM:MeOH 20:1 v/v) to obtain **Ru-3PMI-Ad** as a red-orange solid.

Yield 88%. ^{1}H NMR (400 MHz, $(CD_3)_2CO$): δ 9.08−9.02 (m, 1H), 8.96−8.76 (m, 6H), 8.70−8.63 (m, 1H), 8.58−8.33 (m, 14H), 7.98−7.80 (m, 5H), 7.76−7.78 (m, 2H), 7.67−7.62 (m, 1H), 7.59−7.55 (m, 1H), 7.41−7.31 (m, 1H), 4.98−4.90 (m, 1H), 1.93 (sb, 3H), 1.83−1.46 (m, 12H), 1.32 (sb, 2H) ppm. ^{13}C NMR (100 MHz, $(CD_3)_2CO$) shown in Figure S30. HR-MS: calcd for $C_{70}H_{51}N_7O_2Ru$ $[M]^{2+}$ 561.65779, found $[M]^{2+}$ 561.65689.

Electronic Absorption, Fluorescence, Infrared, and NMR Measurements. Electronic absorption spectroscopy was performed by using a PerkinElmer Lambda 6 spectrophotometer in a 1 × 1 cm quartz cuvette. Fluorescence spectra and measurements of the phosphorescence signal of $^1O_2$ were carried out on a Horiba FluoroMax Plus spectrofluorometer. Attenuated total reflection infrared (ATR-IR) spectroscopy was measured in ATR mode on a IRAffinity-1S SHIMADZU equipped with the ATR sampling accessory (MIRacleTM PIKE Technologies). The ^{1}H, ^{13}C NMR, COSY, and HSQC spectra were collected with a Bruker 400 MHz spectrometer.

Computational Details. Ab initio calculations within the DFT framework have been performed with the Gaussian16 suite of programs[35] using the B3LYP exchange and correlation functional and the LANL2DZ basis set. The solvent effect (acetonitrile) has been described through polarizable continuum model (PCM).[36] The molecular structures have been optimized with a tight criterion and an improved grid in the numerical evaluation of the integrals INTEGRAL (GRID = 199974). TD-DFT calculations were performed considering 12 singlet and 12 triplet excited states.

Singlet Oxygen Sensitizing Properties. Direct determination of singlet oxygen quantum yields (ϕ_Δ) of ruthenium complexes was obtained through the measurement of the $O_2(^1\Delta_g) \rightarrow {}^3O_2$ phosphorescence signal at 1270 nm, upon irradiation of the dyads at 440 nm in air-saturated acetonitrile solutions. Experiments were run on solutions of RPCs at different concentrations, with the ^{1}MLCT absorbance values within the range of 0.08−0.2, and signals were collected by a N_2 cooled InGaAs photodiode; ϕ_Δ values were obtained by taking $[Ru(phen)_3]Cl_2$ as a reference for $^1O_2$ production. Measurements were performed on a Horiba FluoroMax Plus spectrophotofluorimeter.

Transient Absorption Spectroscopy. The apparatus used for the transient absorption spectroscopy measurements has been described in detail before.[37] Briefly, 40 fs pulses centered at 800 nm were produced by a Ti:sapphire oscillator (Micra-Coherent) coupled with a regenerative amplifier system (Legend-Coherent). The excitation wavelength was set at 400 or 480 nm. The pump pulses at 400 nm were obtained by second harmonic generation of the fundamental laser radiation using a 2 mm thick BBO crystal, while pulses at 480 nm were obtained by frequency mixing the 800 nm radiation with the signal output of a commercial optical parametric amplifier (TOPAS, Light Conversion) in a BBO crystal. The white light probe pulse was generated by focusing a small portion of the fundamental laser radiation on a 3 mm thick CaF_2 window. A portion of the generated white light was sent to the sample through a different path and was used as a reference signal. After passing through the

https://doi.org/10.1021/acs.inorgchem.3c04569
Inorg. Chem. XXXX, XXX, XXX−XXX

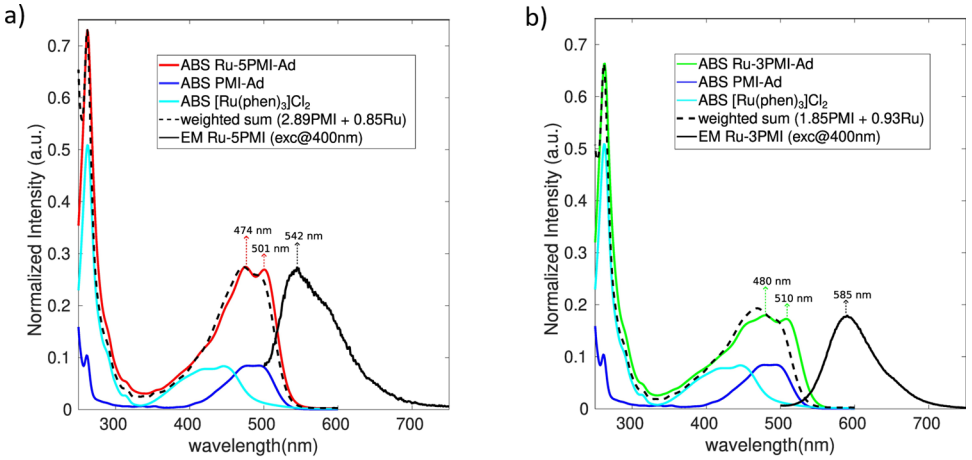

Figure 1. Absorption spectra of compounds **Ru-5PMI-Ad** (red solid line in panel a) and **Ru-3PMI-Ad** (green solid line in panel b) in CH_3CN, together with the ones of PMI-Ad (blue solid line) and $[Ru(phen)_3]Cl_2$ (cyan solid line). The dotted line represents the weighted sum of the absorption spectra of the two moieties that better reproduce the absorption of the dyads. Black solid lines represent the fluorescence spectra of the compounds collected by excitation at 400 nm.

Table 1. Absorption and Fluorescence Maxima ($\lambda_{max}/\lambda_{em}$) of Ru-5PMI-Ad and Ru-3PMI-Ad in Different Media and $^1O_2$ Quantum Yields (φ_Δ) in Acetonitrile[a]

complex	λ_{max}/nm (ε x $10^3/M^{-1}cm^{-1}$) in CH_3CN	λ_{max}/nm (ε x $10^3/M^{-1}cm^{-1}$) in H_2O	λ_{em}/nm in CH_3CN	λ_{em}/nm in H_2O	φ_Δ ($^1O_2$) CH_3CN
$[Ru(phen)_3]Cl_2$	440 (16.2), 262 (101.7)	440 (15.8), 265 (98.3)	590[b,c]	590[b,c]	0.38 ± 0.08
PMI-Ad	485 (16.8)	470 (7.70)	540[b,c]	630[b], 650[c]	0.28 ± 0.06
Ru-5PMI-Ad	500 (53.8), 475 (54.9), 262 (146.1)	480 (34.0), 265 (110.4)	542[b,c]	618[b,c]	0.73 ± 0.06
Ru-3PMI-Ad	510 (34.9), 480 (35.9), 262 (132.1)	500 (20.5), 460 (25.0), 265 (106.2)	585[b], 568[c]	600[b], 590[c]	0.92 ± 0.06

[a]$[Ru(phen)_3]Cl_2$ and PMI-Ad were also considered for comparison. [b]Measured with λ_{exc} = 420 nm. [c]Measured with λ_{exc} = 490 nm.

sample, the white light probe and reference pulses were both directed to a flat field monochromator coupled to a homemade detector. Transient signals were acquired over a time interval spanning up to 1500 ps. The sample was contained in a 2 mm quartz cuvette mounted on a movable holder to minimize photodegradation. Measurements were performed at room temperature. Concentrations were adjusted to an absorbance of 0.9−1.0 OD (for the respective optical path) at the absorption maximum. Before and after the measurements, the integrity of the sample was checked on a PerkinElmer LAMBDA 950 spectrophotometer. The data have been analyzed by global analysis using the software Glotaran.[38]

Measurements of Fluorescence Emission Lifetimes. To measure decay times longer than 1.5 ns, we used the time-correlated single photon counting (TCSPC) setup of a spectrofluorometer FLUOROMAX+ HORIBA. A pulsed LED lamp emitting 1.5 ns pulses at 369 nm with a high repetition rate (1 MHz) was employed as the excitation source. The fluorescence signal decay of the fluorophore was registered along with the light scattered by a pure diffuser, LUDOX, under the same experimental conditions. The special software realized by HORIBA was employed for the analysis of the decay curves, affording the pure fluorescence decay signal, following the deconvolution of the instrumental response of the experimental apparatus.

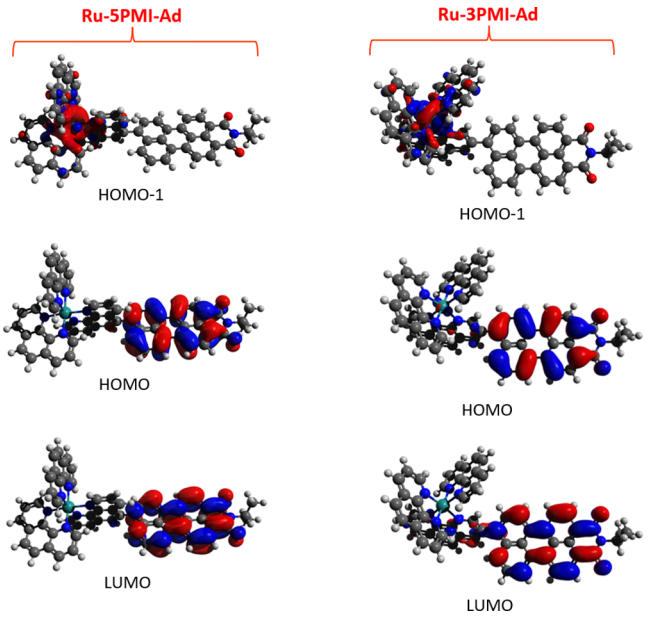

Figure 2. HOMO−1, HOMO, and LUMO orbitals computed at the B3LYP/LanL2DZ level of theory through the Gaussian 16 suite of programs.

RESULTS AND DISCUSSION

Synthesis of Ruthenium Complexes. **Ru-5PMI-Ad** and **Ru-3PMI-Ad** were synthesized by adopting a "*chemistry-on-the-complex*" approach,[39] via the synthetic routes sketched in Scheme 1 and described in detail in the Experimental Section. The polymeric precursor $[Ru(CO)_2Cl_2]_n$ (**1**) was allowed to react with 5-bromo-1,10-phenanthroline (**2a**) or 3-bromo-1,10-phenanthroline (**2b**) in refluxed methanol to obtain *trans*(Cl)-[Ru(5-bromo-1,10-phen)$Cl_2(CO)_2$] (**3a**) or *trans*(Cl)-[Ru(3-bromo-1,10-phen)$Cl_2(CO)_2$] (**3b**), according to procedures reported for analogue complexes.[33] Then, reaction of **3a** and **3b** with two equivalents of phen in 2-methoxyethanol and in the presence of TMAO as a decarbonylation agent, afforded **4a** and **4b**, which were isolated as dihexafluorophosphate salts. Ruthenium complexes were then obtained following Suzuki−Miyaura cross-coupling between these intermediates and the pinacol boronic ester **5**,

https://doi.org/10.1021/acs.inorgchem.3c04569
Inorg. Chem. XXXX, XXX, XXX−XXX

Table 2. $^1O_2$ Quantum Yields (φ_Δ) of Ruthenium Compounds in Air-Saturated Acetonitrile Solutions Determined by Employing Different Excitation Wavelengths (λ_{exc}) in the 440−480 nm Range

λ_{exc}	Ru-5PMI-Ad	Ru-3PMI-Ad
440 nm	0.73 ± 0.06	0.92 ± 0.06
460 nm	0.71 ± 0.06	0.70 ± 0.06
480 nm	0.72 ± 0.06	0.70 ± 0.06

prepared using a previously described synthetic route (see also Supporting Information).[34] This last reaction step was conducted in refluxed DMF/H_2O with $Pd(PPh_3)_4$ as a catalyst and K_2CO_3 as a base, affording, after purification via flash chromatography, **Ru-5PMI-Ad** and **Ru-3PMI-Ad** in high yields of 64 and 88%, respectively. The compounds were fully characterized through ^1H, ^{13}C, COSY and HSQC NMR spectroscopy, FTIR analysis, high-resolution mass spectrometry (HR-MS) (Figures S1−S34, SI), and UV−vis absorption and emission spectroscopy (Figures S46−S47, SI). The intense ν(CO) absorptions in the range 2060−1990 cm^{-1} in the FTIR spectra of intermediates **3a** and **3b** (Figures S5 and S10, ESI) confirmed their *trans*-chloro, *cis*-carbonyl isomerism as, according to literature,[40,41] the ν(CO) vibrations of *cis*(Cl)-*cis*(CO)-[Ru(NN)$(CO)_2Cl_2$] (NN = bidentate ligand) isomers usually occur at lower frequencies (2030−1960 cm^{-1}). Intermediates **4a−b** and complexes **Ru-5PMI-Ad** and **Ru-3PMI-Ad** were isolated as mixtures of diastereoisomers due to the presence of the asymmetrically functionalized phen ligand in the architectures of the heteroleptic complexes.[42] The identity of these compounds was confirmed by the combination of NMR and HR-MS data; in particular, the molecular peaks at 361.00901, 361.00896, 561.65710, and 561.65689 in the HR-MS spectra of **4a**, **4b**, **Ru-5PMI-Ad**, and **Ru-3PMI-Ad**, respectively,are associated with the bipositive charged species $[M\text{-}2PF_6^-]^{2+}$ (m/z = 2, M = **4a**, **4b**, **Ru-5PMI-Ad**, and **Ru-3PMI-Ad**) (see ESI, Figures S15, S21, S27, S33).

Attempts to synthesize the final ruthenium complexes according to "classical" synthetic processes, namely, via the preliminary preparation of the PMI derivatives of phen ligands (Phen-5PMI-Ad and Phen-3PMI-Ad) were also made. However, the competitive phenanthroline coordination to the palladium species formed in the catalytic cycle of the Suzuki−Miyaura coupling reaction resulted in higher reaction times and lower reaction yields, which were in turn also affected by the complicated purification procedures required by the limited solubility of the phenanthroline-PMI-Ad derivatives (paragraph 2, SI). These issues further highlight the higher effectiveness of the "*chemistry-on-the-complex*" approach herein implemented.

Absorption, Fluorescence Behavior, and TD-DFT Calculations. The UV−vis absorption and fluorescence spectra of **Ru-5PMI-Ad** and **Ru-3PMI-Ad** in acetonitrile are shown in Figure 1a,b, together with the weighted sum (dashed black curve) of the absorption spectra of $[Ru(phen)_3]Cl_2$ and the unconjugated PMI-Ad ligand, chosen as reference compounds for the Ru-cores and the appended dye, respectively (see also Chart S2, Supporting Information). The analogue spectra obtained in water are reported in Figure S46 (Supporting Information), whereas the molar extinction coefficients (ε) in the different media are summarized in Table 1. As shown in Figure 1, **Ru-5PMI-Ad** and **Ru-3PMI-Ad** display similar absorption profiles, characterized by an intense band centered at 262 nm, also present in $[Ru(phen)_3]Cl_2$ and mainly ascribable to intraligand $\pi \rightarrow \pi^*$ transitions, plus a broad one in the visible region. This latter band consists in the superposition of two components centered at 474 and 501 nm for **Ru-5PMI-Ad** and at 480 and 510 nm in case of **Ru-3PMI-Ad**, respectively, assigned to the absorption of $[Ru(phen)_3]Cl_2$ and PMI-Ad. For both dyads, the absorption band in the visible region cannot be obtained as the 1:1 sum of the individual components, indicating partial conjugation and ground-state interactions. Figure 1 also shows the emission

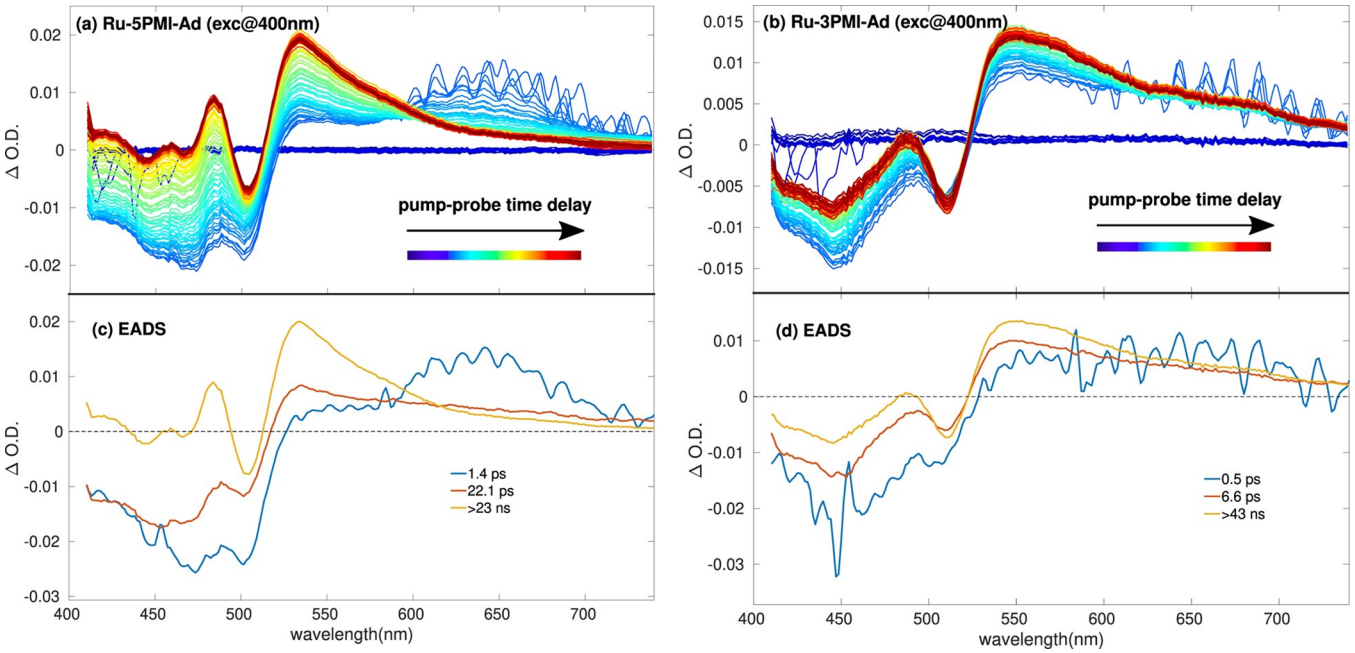

Figure 3. Transient absorption spectra of compounds (a) **Ru-5PMI-Ad** and (b) **Ru-3PMI-Ad** dissolved in CH_3CN and excited at 400 nm. Evolution-associated decay spectra obtained by global analysis for compounds (c) **Ru-5PMI-Ad** and (d) **Ru-3PMI-A**, respectively.

https://doi.org/10.1021/acs.inorgchem.3c04569
Inorg. Chem. XXXX, XXX, XXX−XXX

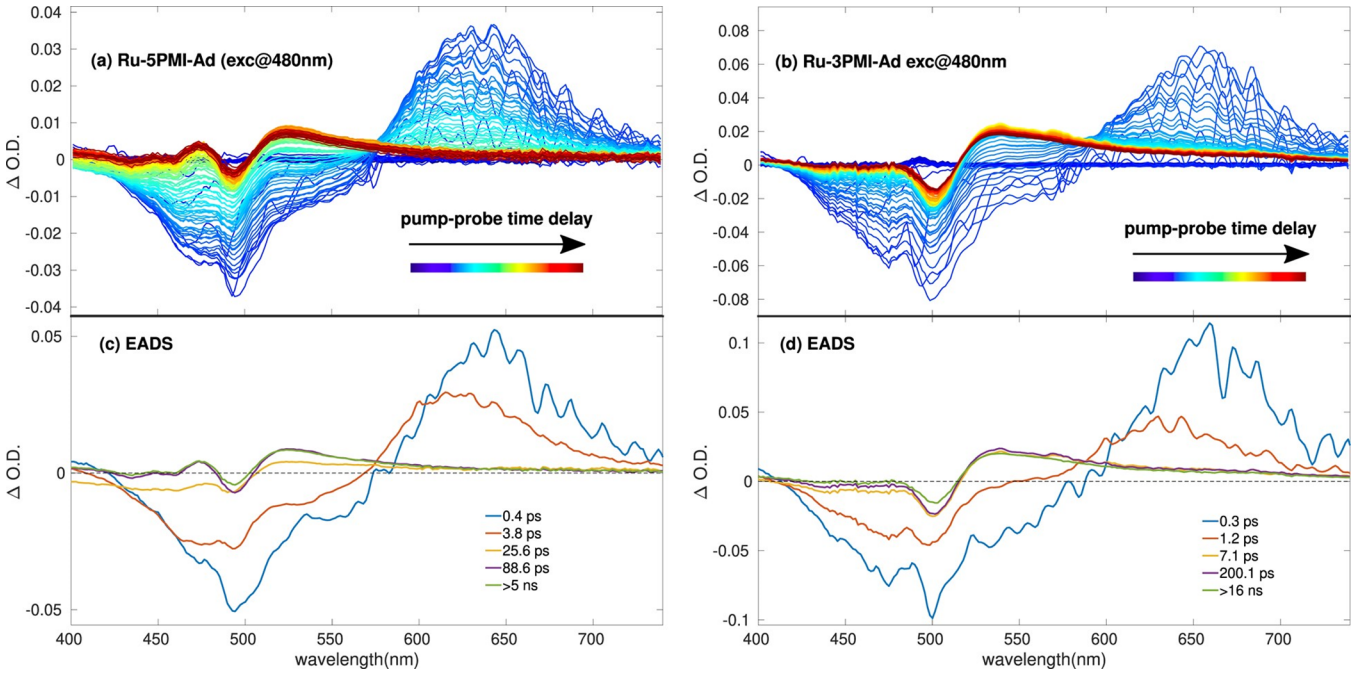

Figure 4. Transient absorption spectra of compounds (a) **Ru-5PMI-Ad** and (b) **Ru-3PMI-Ad** dissolved in CH_3CN and excited at 480 nm. Evolution-associated decay spectra obtained by global analysis for compounds (c) **Ru-5PMI-Ad** and (d) **Ru-3PMI-Ad**, respectively.

Table 3. Time Constants Obtained from Global Analysis of the Kinetic Traces Recorded for Ru-5PMI-Ad and Ru-3PMI-Ad Dissolved in CH_3CN and Excited at 400 and 480 nm

complex	τ_1	τ_2	τ_3	τ_4	τ_5
Ru-5PMI-Ad (λ_{exc} 400 nm)	1.4 ps	22.1 ps	>23 ns		
Ru-3PMI-Ad (λ_{exc} 400 nm)	0.5 ps	6.6 ps	>43 ns		
Ru-5PMI-Ad (λ_{exc} 480 nm)	0.4 ps	3.8 ps	25.6 ps	88.6 ps	>5 ns
Ru-3PMI-Ad (λ_{exc} 480 nm)	0.3 ps	1.2 ps	7.1 ps	200.8 ps	>16 ns

spectra of the metal complexes collected exciting the samples at 400 nm, centered at 542 and 585 nm for **Ru-5PMI-Ad** and **Ru-3PMI-Ad**, respectively. The emission profiles registered in CH_3CN upon excitation at 490 nm and in H_2O at both excitation wavelengths are reported in Figure S47 of SI.

Judging from the absorption spectra of the individual moieties in acetonitrile, excitation at 400 nm is mainly localized on the $Ru(phen)_3$-core; however, the emission spectrum of **Ru-5PMI-Ad**, centered at 542 nm, is very similar to the one of PMI-Ad (Figure S47a, SI), suggesting that energy transfer is occurring between the two moieties. The emission of **Ru-3PMI-Ad** instead is centered at 585 nm and fully reflects the emission spectrum of $[Ru(phen)_3]Cl_2$, indicating that excitation remains localized on the metal center and energy transfer is less efficient. Employing an excitation wavelength (λ_{exc}) of 490 nm, which predominantly excites the PMI-Ad moiety, the emission of **Ru-5PMI-Ad** still reflects the one of PMI-Ad, being centered at 542 nm, while the one of **Ru-3PMI-Ad**, centered at 568 nm, presents contributions from both PMI-Ad and the $Ru(phen)_3$-core, thus indicating partial delocalization over the two moieties (Figure S47b, SI). In water, this trend seems to be preserved, even though the broader spectra collected in this solvent make the interpretation less straightforward (Figure S47c,d, SI). These findings indicate that the different positions for the PMI-Ad substitution in the Ru(II)-based dyads have a certain influence on their electronic properties, with more efficient energy transfer occurring for **Ru-5PMI-Ad**.

To better analyze the different spectroscopic behaviors of the two compounds, TD-DFT calculations have been performed. As shown in Figure 2, the main orbital contributions to the electronic transitions can be ascribed to HOMO−1, HOMO, and LUMO orbitals. HOMO−1 in both systems extends exclusively on the central ruthenium core, whereas both HOMO and LUMO are more delocalized in **Ru-3PMI-Ad** relative to **Ru-5PMI-Ad**. It is important to note that the excitation of **Ru-5PMI-Ad** or **Ru-3PMI-Ad**, corresponds mainly to a HOMO/LUMO transition in both cases, both for a singlet (allowed) and triplet (prohibited) state. Excitation leads, in the first case, to a LUMO whose electronic distribution is straightly localized on PMI-Ad, and thus justifies the emission profile in Figure 1a, closely resembling that of the free PMI-Ad ligand. Instead, in the case of **Ru-3PMI-Ad**, the LUMO orbital is delocalized on both the ruthenium center and PMI-Ad, which is in line with the hybrid character of the emission spectra in Figure 1b. This is also in good agreement with the results of transient absorption analysis (*vide infra*).

Singlet Oxygen Sensitizing Properties. The singlet oxygen sensitizing properties of the two dyads were assessed by direct measurement of the $^1O_2$ phosphorescence at 1270 nm upon irradiation of air-saturated acetonitrile solutions of the compounds at 440 nm. As shown in Table 1, **Ru-5PMI-Ad** and **Ru-3PMI-Ad** feature potent sensitizing capabilities, with quantum yields for $^1O_2$ generation (φ_Δ) of 0.73 ± 0.06 and 0.92 ± 0.06, respectively. Notably, these values are up to 2.4- or 3.3-fold higher if compared to the reference compound $[Ru(phen)_3]Cl_2$ (φ_Δ = 0.38 ± 0.06)[43] or the unbounded chromophore (φ_Δ(PMI-Ad) = 0.28 ± 0.06). This clearly demonstrates that combining the classical $Ru(phen)_3$-core with

https://doi.org/10.1021/acs.inorgchem.3c04569
Inorg. Chem. XXXX, XXX, XXX−XXX

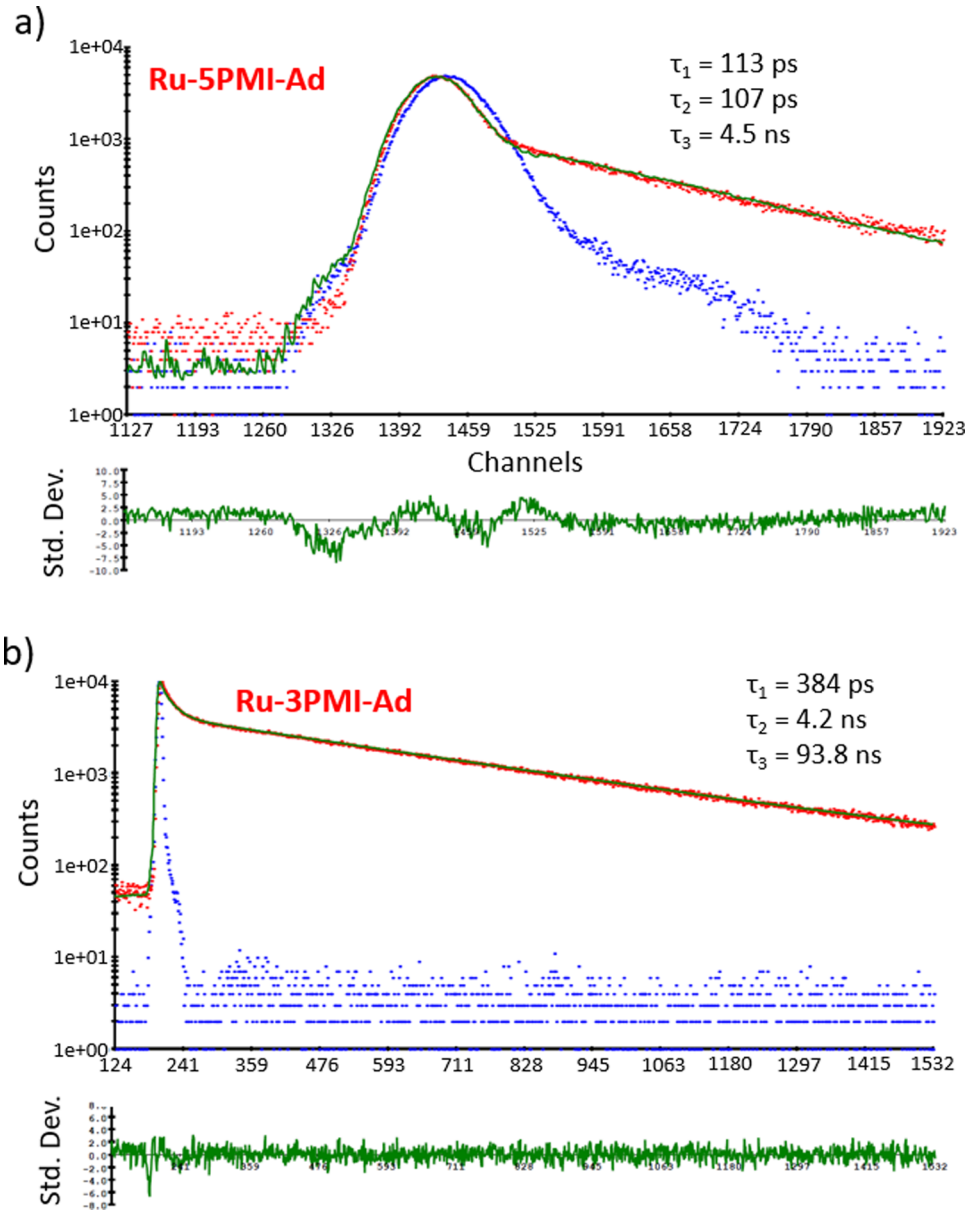

Figure 5. (a) TCSPC signals at 542 nm of **Ru-5PMI-Ad** (red dots, a) and at 590 nm of **Ru-3PMI-Ad** (red dots, b) along with the LUDOX scatterer (blue dots) and (b) TCSPC signal at 590 nm of **Ru-3PMI-Ad** (red dots) and of the LUDOX scatterer (blue dots). Air-equilibrated acetonitrile solutions, green lines, are the best fit curves obtained by deconvolving the prompt signals from the fluorescence ones. Lower panels report the residual of the fits, highlighting the higher quality obtained for **Ru-5PMI-Ad**. λ_{exc} = 369 nm.

differently functionalized PMI-Ad ligands is a powerful strategy to endow the resulting compounds with augmented sensitizing properties.

It can also be noted that the lower φ_{Δ} value was obtained for **Ru-5PMI-Ad**, namely, the compound featuring the highest energy transfer and, so, the lowest orbital delocalization between the Ru(phen)$_3$-core and PMI-Ad relative to **Ru-3PMI-Ad** (*vide supra*); this suggests that a higher electronic delocalization between the PMI-Ad chromophore and the Ru(phen)$_3$ center has a positive effect on the sensitizing capabilities of these metal complexes.

The singlet oxygen sensitizing properties of ruthenium complexes were also investigated by employing different excitation wavelengths (λ_{exc}), namely, 440, 460, and 480 nm; the obtained results are reported in Table 2. As shown in the Table, $^1O_2$ generation by **Ru-5PMI-Ad** was not greatly affected by the excitation wavelength. Instead, significant variations were displayed by **Ru-3PMI-Ad**, as witnessed by a decrease of *c.ca* 20% in the $^1O_2$ quantum yield when passing from λ_{exc} of 440 to 480 nm.

Such greater susceptibility of **Ru-3PMI-Ad** to the excitation wavelength would be in line with its lower energy transfer and, so, higher orbital delocalization if compared to **Ru-5PMI-Ad**. Moreover, the lower φ_{Δ} value registered when using λ_{exc} of 480 nm (φ_{Δ} = 0.70), namely, a radiation which is more localized on the PMI-Ad ligand rather than the Ru(phen)$_3$-core, would unveil that increasing the localization on the PMI-Ad appended chromophore is slightly detrimental to the sensitizing capabilities of ruthenium complexes.

Transient Absorption Spectroscopy and Emission Lifetime Measurements. To verify the formation of triplet states and determine the rate of intersystem crossing, we

https://doi.org/10.1021/acs.inorgchem.3c04569
Inorg. Chem. XXXX, XXX, XXX−XXX

Scheme 2. Diagram of the Energy Levels and Relaxation Pathways Involved in the Electronic Transitions of Ruthenium Compounds[a]

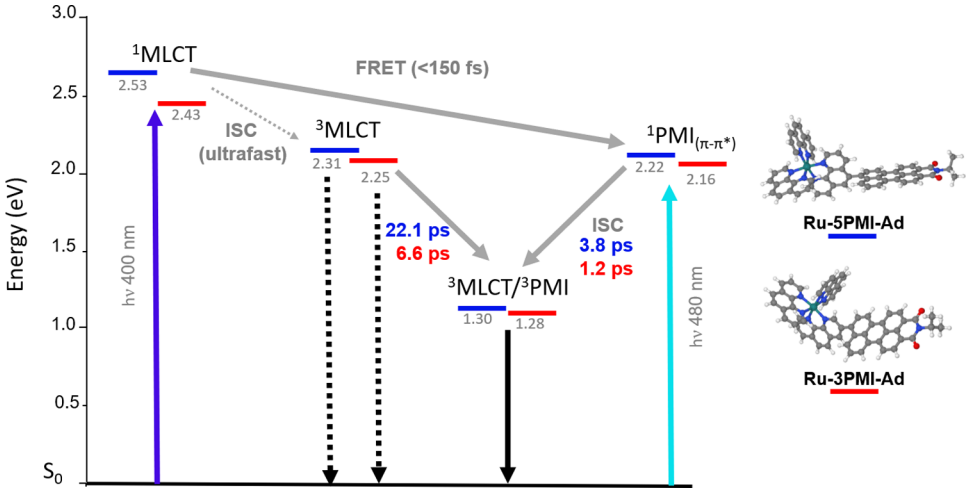

[a]Energy levels computed with the TD-DFT method at B3LYP/LANL2DZ level of theory. The time scales of the photoinduced relaxation processes are obtained from transient absorption measurements.

measured the transient spectra of **Ru-3PMI-Ad** and **Ru-5PMI-Ad** in CH_3CN upon excitation at both 400 and 480 nm. The data were analyzed using a global analysis procedure,[44] which consists in the simultaneous fit of the kinetic traces registered in the entire analyzed spectral interval with a combination of exponential decay functions. We applied a linear unidirectional decay scheme, obtaining both the kinetic constants associated with the dynamic evolution of the probed system and the corresponding spectral components, termed evolution-associated difference spectra (EADS). The transient spectra registered with λ_{exc} = 400 nm are reported in Figure 3a,b, while Figure 3c,d shows the corresponding EADS obtained from global fitting.

For **Ru-5PMI-Ad,** the spectra registered immediately after excitation present a quite broad negative signal centered at 475 nm and a positive band centered at 650 nm. The negative band can be associated with ground-state bleaching (GSB) since its spectral position corresponds to the absorption band of the sample. The assignment of the positive excited-state absorption (ESA) band can be made by comparison with the transient spectra registered for the individual components reported in Supporting Information (Figure S48). Since a similar ESA band is observed in the transient spectra of the isolated PMI-Ad moiety, the band centered at 650 nm can be interpreted as a signature of the singlet excited state of this chromophore. In the transient spectra of **Ru-5PMI-Ad,** the ESA appears broader if compared to that of the isolated PMI-Ad, possibly reflecting a contribution of the $Ru(phen)_3$-moiety, which indeed presents a broad ESA in the 520−580 nm region (Figure S48, Supporting Information). It is known that RPCs undergo ultrafast intersystem crossing, populating triplet states on a subpicosecond time scale.[45] Because we do not observe any fast spectral evolution when measuring the transient spectra of the isolated $Ru(phen)_3$-moiety, which would be indicative of ISC, we assume that the triplet state of the metal complex is populated on a time scale faster than our time resolution. The observation of the ESA band assigned to PMI-Ad in the transient spectra of **Ru-5PMI-Ad** implies either an ultrafast energy transfer from the $Ru(phen)_3$-core to PMI-Ad, occurring on a time scale below the time resolution of the measurement and before the ISC of the $Ru(phen)_3$-core (since the ESA of PMI-Ad is due to its bright $^1\pi\pi$ state), or a partial direct excitation of the PMI-Ad moiety at 400 nm. Global analysis of the transient data of **Ru-5PMI-Ad** indicates that spectral evolution occurs on a quite fast time scale. Indeed, looking at the evolution between the first (blue) EADS and second (red) EADS reported in Figure 3c, occurring in 1.4 ps, we observed the recovery of the PMI-Ad singlet ESA centered at 650 nm and a partial decrease of the bleaching signal. The decay of the 650 nm ESA possibly indicates localization of the excitation on the metal center, which should already be in the triplet state on this time scale. The spectrum further evolves on the following 22 ps time scale: on this time scale, we observe a further recovery of the broad GSB signal, which is replaced by a narrow negative band peaking at about 500 nm and the development of a positive band centered at 540 nm. The final spectral component (yellow line in Figure 3c) is very long-lived and does not decay on the time scale of our measurement (1.5 ns).

The comparison of the spectral shape of the long-lived EADS with literature data[46,47] allows to assign this spectral component as the triplet state of PMI-Ad, which is most probably populated via triplet energy transfer from the $Ru(phen)_3$-core in about 20 ps.

For **Ru-3PMI-Ad** (Figure 3b,d), the contribution of the 650 nm ESA band assigned to the singlet state of PMI-Ad at the short time scale is less evident, and the spectral evolution observed within the investigated time scale appears more limited. In this case, the long living species, populated in about 6.6 ps, appears as the convolution of the triplet states of both the $Ru(phen)_3$-core and PMI-Ad (see Supporting Information for further details). Indeed, the long-lived EADS (yellow line in Figure 3d) presents two negative bands, peaked at 450 nm, similar to the bleaching observed for the isolated $Ru(phen)_3$, and at 510 nm, indicative of the PMI-Ad triplet. Furthermore, the positive signal centered at about 540 nm is broader than what is observed for **Ru-5PMI-Ad** because of the contribution from the $Ru(phen)_3$-triplet state absorption (Figure S48, Supporting Information). This suggests that the final triplet state reached by the dyad is partially delocalized on both

https://doi.org/10.1021/acs.inorgchem.3c04569
Inorg. Chem. XXXX, XXX, XXX−XXX

components. It is worth noticing that for both compounds there is no evidence for the formation of a charge-separated state prior to triplet formation so that a charge recombination-induced ISC mechanism can be excluded.

Transient absorption measurements have also been repeated exciting the compounds at 480 nm, namely, by using an excitation wavelength which is mainly localized on the PMI-Ad moiety; the transient absorption spectra and respective EADS are reported in Figure 4. For both samples, the spectra registered soon after excitation show a broad GSB signal, respectively, centered at 490 nm in the case of **Ru-5PMI-Ad** (Figure 4a) and 500 nm for **Ru-3PMI-Ad** (Figure 4b). Furthermore, an ESA band, respectively centered at 620 and 650 nm, is observed, assigned to the singlet ESA of the PMI-Ad moiety. The evolution of the transient signal is very fast for both dyads. Indeed, on a subpicosecond time scale (evolution from the blue to red EADS in Figure 4c,d), we observe the partial recovery of the GSB signal and the decrease in intensity and blue shift of the ESA band. We attribute this evolution to a fast excited-state relaxation, possibly induced by solvation.

The appearance of the transient spectra completely changes on the following evolution, occurring in about 4 ps in the case of **Ru-5PMI-Ad** and 1 ps for **Ru-3PMI-Ad**. On this time scale, the broad ESA band attributed to the PMI-Ad completely recovers, while a less intense ESA peaked at 540 nm develops. Moreover, the broad GSB signal observed soon after excitation is replaced by a narrow and less intense signal peaked at about 500 nm.

Comparison with literature data[46,47] and with measurements performed upon excitation at 400 nm indicates the occurrence of ultrafast ISC in both systems, being the spectral shape observed on this time scale very similar to the long living signal already observed at different excitation conditions (Figure 4) and assigned to a triplet state mostly localized on the PMI-Ad chromophore. The transient signal does not significantly evolve on the following time scale, although different time constants are extracted from the analysis to allow for a correct fit of the kinetic traces. All of the following evolution can be interpreted in terms of vibrational and solvent-induced relaxation of the triplet state.

Selected kinetic traces, reported in Figure S52 (Supporting Information), further elucidate that ISC is fast for both compounds but relatively faster in the case of **Ru-3PMI** at both excitation wavelengths.

The kinetic constants extracted from global analysis for the measurements performed in CH_3CN at different excitation wavelengths are summarized in Table 3. Although the last time constant retrieved from global analysis at both the excitation wavelengths is affected by a significant error, the lifetime of the final triplet state reached by the two compounds being much longer than the investigated time scale, the results of the global fit suggest a longer lifetime in the case of **Ru-3PMI-Ad** as compared with **Ru-5PMI-Ad**. This finding is in line with higher singlet oxygen QY measured for this compound. Transient measurements have been further repeated by dissolving the dyads in H_2O at both excitation wavelengths (Figures S49 and S50, Supporting Information). Although the solubility of the compounds is lower in this solvent and triplet formation appears less efficient as compared with what is observed in CH_3CN, these measurements indicate that the compounds could be effectively employed in a biologically relevant environment. Looking at the results reported in Supporting Information, the triplet state appears delocalized over the two moieties in water. Moreover, the relaxation processes are slower than in CH_3CN (kinetic traces in H_2O reported in Figure S52, Supporting Information). The time constants retrieved from the analysis of the data recorded in H_2O are reported in Table S1 in the Supporting Information.

Lastly, the emission lifetimes (τ) of both dyads were also measured. As shown in Figure 5 (see also Figure S53), because of experimental constraints, emission lifetimes were recorded with excitation at 369 nm, mainly localized on the $Ru(phen)_3$-moiety. **Ru-5PMI-Ad** displays a quite fast emission decay, preventing us to obtain a good experimental fit, as also evidenced by the small mismatch between the prompt signal (due to the perfect scatterer) and the emission signal of the complex (Figure 5a). A good fit of the emission decay curve is instead obtained for **Ru-3PMI-Ad** by using three exponential functions (as noticed in Figure 5b). The lifetimes (τ) obtained by the analysis of the emission decay measurements further support the observation retrieved from transient absorption spectroscopy and the theoretical analysis. Indeed, the highest τ values are registered for **Ru-3PMI-Ad** complex, which presents a more delocalized triplet state. The long luminescence lifetime of this compound can probably be attributed to the emission contribution of the metal center. In the case of **Ru-5PMI-Ad**, whose triplet state is rather strongly localized on the PMI-Ad moiety, the luminescence is extremely week, preventing a good estimate of the emission lifetime.

These results are also in agreement with the different singlet oxygen sensitizing properties of the two metal complexes and underlie once again that the highest orbital delocalization exhibited by **Ru-3PMI-Ad** is beneficial to increase the triplet state lifetime of this compound.

To give an overview of the photophysical processes occurring in the two dyads upon photoexcitation, we report in Scheme 2 a summary of the main relaxation paths and the energy of the various excited states involved in the photodynamics of the dyads, as obtained by DFT computations.

CONCLUSIONS

To summarize, herein we describe two novel RPC-based dyads, **Ru-3PMI-Ad** and **Ru-5PMI-Ad**, featuring a dissymmetric perylene monoimide chromophore (PMI-Ad) linked to the 3- or 5-positions of the Ru(II)-coordinated phen ligands via a single C−C bond. The synthesis was accomplished by adopting a "*chemistry-on-the-complex*" approach, namely, by linking the PMI-based chromophores directly on the Ru(II)-coordinated phen units, leading to improved outcomes if compared to the more "classically employed" synthetic routes. Then we performed a comprehensive chemical-physical investigation of the obtained systems, demonstrating that combining the $Ru(phen)_3$-core with PMI-Ad ligands represents a powerful strategy to construct potent photosensitizers, as testified by φ_Δ values ranging from 0.70 to 0.92, among, to the best of our knowledge, the highest reported in the literature for RPCs. The idea of linking organic chromophores to metal centers with the aim of increasing the triplet lifetime of the resulting dyads is often referred in literature as the "*reservoir effect*".[48−50] The presence of an organic chromophore whose triplet state is close in energy to the ^{3}MLCT of the metal center would prolong the lifetime of the overall dyad, being $^3\pi\pi$ state of the chromophore intrinsically long-lived because of the forbidden nature of the $^3\pi\pi \rightarrow {}^1\pi\pi$ transition. In the case of our compounds, the low-lying triplet state populated with high efficiency is predominantly localized on

https://doi.org/10.1021/acs.inorgchem.3c04569
Inorg. Chem. XXXX, XXX, XXX−XXX

the organic moiety; nevertheless, some contribution from the metal center is observed, with the amount of electron delocalization dependent on the chromophore positioning. Summarizing the observations based on time-resolved absorption and emission spectroscopy as well as from the theoretical analysis, we conclude that both **Ru-3PMI-Ad** and **Ru-5PMI-Ad** undergo very fast and efficient intersystem crossing, justifying their excellent singlet oxygen sensitizing properties. Importantly, the overall chemical−physical behavior of the two dyads (singlet oxygen sensitization, absorption and emission profiles, etc.) appears to be the result of a subtle modulation of energy transfer and electron delocalization between the $Ru(phen)_3$-cores and PMI-Ad ligands, which is in turn imparted by the different substitution patterns of the PMI-Ad chromophore. In particular, placing the PMI-Ad in the 3-position of **Ru-3PMI-Ad** is clearly advantageous for maximizing the singlet oxygen production by virtue of increased electron delocalization and prolonged triplet state lifetime, possibly arising from the contribution of the metal center.

In conclusion, this work highlights the potential arising from the combination of RPCs with PMI-based chromophores in designing powerful dyads as promising candidates for PDT. It especially proves that the C−C decoration with PMI-based chromophores, along with the position of their functionalization, subtly affects the electronic properties of these compounds, allowing us to obtain in both cases optimal performances.

■ ASSOCIATED CONTENT

Supporting Information

The Supporting Information is available free of charge at https://pubs.acs.org/doi/10.1021/acs.inorgchem.3c04569.

^1H, ^{13}C, $^1H^1H$ COSY, $^1H^{13}C$ HSQC NMR spectra of compounds; HR-MS spectra of **4a**, **4b**, **Ru-5PMI-Ad**, **Ru-3PMI-Ad**, Pinacolylboronate-PMI-Ad, Phen-5PMI-Ad, and Phen-3PMI-Ad; synthetic procedure for the obtaining of Phen-5PMI-Ad and Phen-3MPI-Ad; absorption and fluorescence spectra of ruthenium compounds; transient absorption spectra of ruthenium compounds in different media and exciting at 400 or 480 nm; kinetics traces reckoned for ruthenium compounds; and time constants determined by analysis of kinetic traces for **Ru-3PMI-Ad** and **Ru-5PMI-Ad** (PDF)

■ AUTHOR INFORMATION

Corresponding Authors

Luca Conti − *Department of Chemistry "Ugo Schiff", University of Florence, Sesto Fiorentino (FI) 50019, Italy;* orcid.org/0000-0002-0402-1293; Email: luca.conti@unifi.it

Mariangela Di Donato − *European Laboratory for Non-Linear Spectroscopy (LENS), Sesto Fiorentino (FI) 50019, Italy; CNR-ICCOM, Sesto Fiorentino (FI) 50019, Italy;* orcid.org/0000-0002-6596-7031; Email: didonato@lens.unifi.it

Authors

Gina Elena Giacomazzo − *Department of Chemistry "Ugo Schiff", University of Florence, Sesto Fiorentino (FI) 50019, Italy*

Sandra Doria − *European Laboratory for Non-Linear Spectroscopy (LENS), Sesto Fiorentino (FI) 50019, Italy; CNR-ICCOM, Sesto Fiorentino (FI) 50019, Italy;* orcid.org/0000-0002-9440-1643

Andrea Revilla-Cuesta − *Department of Chemistry, University of Burgos, Burgos 09001, Spain*

Nicola De Monte − *Department of Chemistry "Ugo Schiff", University of Florence, Sesto Fiorentino (FI) 50019, Italy*

Marco Pagliai − *Department of Chemistry "Ugo Schiff", University of Florence, Sesto Fiorentino (FI) 50019, Italy;* orcid.org/0000-0003-0240-161X

Giangaetano Pietraperzia − *Department of Chemistry "Ugo Schiff", University of Florence, Sesto Fiorentino (FI) 50019, Italy; European Laboratory for Non-Linear Spectroscopy (LENS), Sesto Fiorentino (FI) 50019, Italy;* orcid.org/0000-0001-8280-1052

Barbara Valtancoli − *Department of Chemistry "Ugo Schiff", University of Florence, Sesto Fiorentino (FI) 50019, Italy*

Tomás Torroba − *Department of Chemistry, University of Burgos, Burgos 09001, Spain;* orcid.org/0000-0002-5018-4173

Claudia Giorgi − *Department of Chemistry "Ugo Schiff", University of Florence, Sesto Fiorentino (FI) 50019, Italy;* orcid.org/0000-0003-1240-2405

Complete contact information is available at: https://pubs.acs.org/10.1021/acs.inorgchem.3c04569

Author Contributions

The manuscript was written through contributions of all authors. All authors have given approval to the final version of the manuscript.

Notes

The authors declare no competing financial interest.

■ ACKNOWLEDGMENTS

The publication was made by a researcher with a research contract cofunded by the European Union—PON Research and Innovation 2014−2020 in accordance with Article 24, paragraph 3a), of Law No. 240 of December 30, 2010, as amended, and Ministerial Decree No. 1062 of August 10, 2021. The authors also thank Ministerio de Ciencia e Innovación of Spain (Grants PDC2022-133955-I00 and PID2022-142318NB-I00) for financial support.

■ ABBREVIATIONS

PDT=photodynamic therapy; RPCs=ruthenium polypyridyl complexes; phen=phenanthroline; TMAO=*N*,*N*-dimethylmethanamine *N*-oxide; 5PMI=*N*-(2-adamantyl-ethylamine)-9-(5-phenanthroline)-3,4-perylenemonoimide; 3PMI=*N*-(2-adamantyl-ethylamine)-9-(3-phenanthroline)-3,4-perylenemonoimide; PMI=(*N*-(1-(1-adamantyl)ethyl)perylene-3,4-dicarboxylmonoimide); dppf=[1,1′-bis(diphenylphosphino)ferrocene]-palladium(II)dichloride; DABCO=1,4-diazabiciclo[2.2.2]octane

■ REFERENCES

(1) Monro, S.; Colón, K. L.; Yin, H.; Roque, J.; Konda, P.; Gujar, S.; Thummel, R. P.; Lilge, L.; Cameron, C. G.; McFarland, S. A. Transition Metal Complexes and Photodynamic Therapy from a Tumor-Centered Approach: Challenges, Opportunities, and Highlights from the Development of TLD1433. *Chem. Rev.* **2019**, *119* (2), 797−828.

(2) Smith, C. B.; Days, L. C.; Alajroush, D. R.; Faye, K.; Khodour, Y.; Beebe, S. J.; Holder, A. A. Photodynamic Therapy of Inorganic Complexes for the Treatment of Cancer. *Photochem. Photobiol.* **2022**, *98*, 17−41.
(3) Conti, L.; Ciambellotti, S.; Giacomazzo, G. E.; Ghini, V.; Cosottini, L.; Puliti, E.; Severi, M.; Fratini, E.; Cencetti, F.; Bruni, P.; Valtancoli, B.; Giorgi, C.; Turano, P. Ferritin Nanocomposites for the Selective Delivery of Photosensitizing Ruthenium-Polypyridyl Compounds to Cancer Cells. *Inorg. Chem. Front.* **2022**, *9* (6), 1070−1081.
(4) Conti, L.; Mengoni, A.; Giacomazzo, G. E.; Mari, L.; Perfetti, M.; Fagorzi, C.; Sorace, L.; Valtancoli, B.; Giorgi, C. Exploring the Potential of Highly Charged Ru(II)- and Heteronuclear Ru(II)/Cu(II)-Polypyridyl Complexes as Antimicrobial Agents. *J. Inorg. Biochem.* **2021**, *220*, No. 111467.
(5) Giacomazzo, G. E.; Conti, L.; Fagorzi, C.; Pagliai, M.; Andreini, C.; Guerri, A.; Perito, B.; Mengoni, A.; Valtancoli, B.; Giorgi, C. Ruthenium(II) Polypyridyl Complexes and Metronidazole Derivatives: A Powerful Combination in the Design of Photoresponsive Antibacterial Agents Effective under Hypoxic Conditions. *Inorg. Chem.* **2023**, *62* (20), 7716−7727.
(6) Giacomazzo, G. E.; Conti, L.; Guerri, A.; Pagliai, M.; Fagorzi, C.; Sfragano, P. S.; Palchetti, I.; Pietraperzia, G.; Mengoni, A.; Valtancoli, B.; Giorgi, C. Nitroimidazole-Based Ruthenium(II) Complexes: Playing with Structural Parameters to Design Photostable and Light-Responsive Antibacterial Agents. *Inorg. Chem.* **2022**, *61* (18), 6689−6694.
(7) Shum, J.; Leung, P. K.-K.; Lo, K. K.-W. Luminescent Ruthenium(II) Polypyridine Complexes for a Wide Variety of Biomolecular and Cellular Applications. *Inorg. Chem.* **2019**, *58* (4), 2231−2247.
(8) Conti, L.; Macedi, E.; Giorgi, C.; Valtancoli, B.; Fusi, V. Combination of Light and Ru(II) Polypyridyl Complexes: Recent Advances in the Development of New Anticancer Drugs. *Coord. Chem. Rev.* **2022**, *469*, No. 214656.
(9) Chettri, A.; Roque, J. A.; Schneider, K. R. A.; Cole, H. D.; Cameron, C. G.; McFarland, S. A.; Dietzek, B. It Takes Three to Tango: The Length of the Oligothiophene Chain Determines the Nature of the Long-Lived Excited State and the Resulting Photocytotoxicity of a Ruthenium(II) Photodrug. *ChemPhotoChem.* **2021**, *5*, 421−425.
(10) Giacomazzo, G. E.; Schlich, M.; Casula, L.; Galantini, L.; Del Giudice, A.; Pietraperzia, G.; Sinico, C.; Cencetti, F.; Pecchioli, S.; Valtancoli, B.; Conti, L.; Murgia, S.; Giorgi, C. Ruthenium(II) Polypyridyl Complexes with π-Expansive Ligands: Synthesis and Cubosome Encapsulation for Photodynamic Therapy of Non-Melanoma Skin Cancer. *Inorg. Chem. Front.* **2023**, *10* (10), 3025−3036.
(11) Zhou, Q. X.; Lei, W. H.; Chen, J. R.; Li, C.; Hou, Y. J.; Wang, X. S.; Zhang, B. W. A New Heteroleptic Ruthenium(II) Polypyridyl Complex with Long-Wavelength Absorption and High Singlet-Oxygen Quantum Yield. *Chem. - A Eur. J.* **2010**, *16*, 3157−3165.
(12) Lincoln, R.; Kohler, L.; Monro, S.; Yin, H.; Stephenson, M.; Zong, R.; Chouai, A.; Dorsey, C.; Hennigar, R.; Thummel, R. P.; McFarland, S. A. Exploitation of Long-Lived 3IL Excited States for Metal-Organic Photodynamic Therapy: Verification in a Metastatic Melanoma Model. *J. Am. Chem. Soc.* **2013**, *135* (45), 17161−17175.
(13) Ford, W. E.; Rodgers, M. A. J. Reversible Triplet-Triplet Energy Transfer within a Covalently Linked Bichromophoric Molecule. *J. Phys. Chem.* **1992**, *96* (7), 2917−2920.
(14) Murata, K.; Araki, M.; Inagaki, A.; Akita, M. Syntheses, Photophysical Properties, and Reactivities of Novel Bichromophoric Pd Complexes Composed of Ru(II)-Polypyridyl and Naphthyl Moieties. *Dalt. Trans.* **2013**, *42* (19), 6989.
(15) Nomula, R.; Wu, X.; Zhao, J.; Munirathnam, N. R. Photodynamic Effect of Light-Harvesting, Long-Lived Triplet Excited State Ruthenium(II)-Polyimine-Coumarin Complexes: DNA Binding, Photocleavage and Anticancer Studies. *Mater. Sci. Eng., C* **2017**, *79*, 710−719.
(16) Tyson, D. S.; Henbest, K. B.; Bialecki, J.; Castellano, F. N. Excited State Processes in Ruthenium(II)/Pyrenyl Complexes Displaying Extended Lifetimes. *J. Phys. Chem. A* **2001**, *105* (35), 8154−8161.
(17) Monro, S.; Scott, J.; Chouai, A.; Lincoln, R.; Zong, R.; Thummel, R. P.; McFarland, S. A. Photobiological Activity of Ru(II) Dyads Based on (Pyren-1-Yl)Ethynyl Derivatives of 1,10-Phenanthroline. *Inorg. Chem.* **2010**, *49* (6), 2889−2900.
(18) Busto, N.; Romero, D. C.; Revilla-Cuesta, A.; Abajo, I.; Cuevas, J. V.; Rodríguez, T.; García, B.; Torroba, T. Synthesis of Water-Soluble Hemicoronenediimides by Photocyclization of Perylenediimides: Turn-on Fluorescent Probes in Water by Complexation with Cucurbit[7]Uril or Binding to G-Quadruplex Motifs. *Dyes Pigm.* **2022**, *205*, No. 110557.
(19) Calvo-Gredilla, P.; García-Calvo, J.; Cuevas, J. V.; Torroba, T.; Pablos, J. L.; García, F. C.; García, J. M.; Zink-Lorre, N.; Font-Sanchis, E.; Sastre-Santos, Á.; Fernández-Lázaro, F. Solvent-Free Off−On Detection of the Improvised Explosive Triacetone Triperoxide (TATP) with Fluorogenic Materials. *Chem. - A Eur. J.* **2017**, *23*, 13973−13979.
(20) García-Calvo, V.; Cuevas, J. V.; Barbero, H.; Ferrero, S.; Álvarez, C. M.; González, J. A.; Díaz de Greñu, B.; García-Calvo, J.; Torroba, T. Synthesis of a Tetracorannulene-Perylenediimide That Acts as a Selective Receptor for C 60 over C 70. *Org. Lett.* **2019**, *21* (15), 5803−5807.
(21) Amati, A.; Natali, M.; Indelli, M. T.; Iengo, E.; Würthner, F. Photoinduced Energy- and Electron-Transfer Processes in a Side-to-Face RuII-Porphyrin/Perylene-bisimide Array. *ChemPhysChem* **2019**, *20* (17), 2195−2203.
(22) Dubey, R. K.; Niemi, M.; Kaunisto, K.; Stranius, K.; Efimov, A.; Tkachenko, N. V.; Lemmetyinen, H. Excited-State Interaction of Red and Green Perylene Diimides with Luminescent Ru(II) Polypyridine Complex. *Inorg. Chem.* **2013**, *52* (17), 9761−9773.
(23) Salomé Rodríguez-Morgade, M.; Torres, T.; Atienza-Castellanos, C.; Guldi, D. M. Supramolecular Bis(Rutheniumphthalocyanine)-Perylenediimide Ensembles: Simple Complexation as a Powerful Tool toward Long-Lived Radical Ion Pair States. *J. Am. Chem. Soc.* **2006**, *128* (47), 15145−15154.
(24) Gunderson, V. L.; Krieg, E.; Vagnini, M. T.; Iron, M. A.; Rybtchinski, B.; Wasielewski, M. R. Photoinduced Singlet Charge Transfer in a Ruthenium(II) Perylene-3,4:9,10-Bis(Dicarboximide) Complex. *J. Phys. Chem. B* **2011**, *115* (23), 7533−7540.
(25) Kodama, K.; Kobayashi, A.; Hirose, T. Synthesis and Spectral Properties of Ruthenium(II) Complexes Based on 2,2′-Bipyridines Modified by a Perylene Chromophore. *Tetrahedron Lett.* **2013**, *54* (40), 5514−5517.
(26) Santos, E. R. D.; Pina, J.; Venâncio, T.; Serpa, C.; Martinho, J. M. G.; Carlos, R. M. Photoinduced Energy and Electron-Transfer Reactions by Polypyridine Ruthenium(II) Complexes Containing a Derivatized Perylene Diimide. *J. Phys. Chem. C* **2016**, *120* (40), 22831−22843.
(27) Schulze, M.; Steffen, A.; Würthner, F. Near-IR Phosphorescent Ruthenium(II) and Iridium(III) Perylene Bisimide Metal Complexes. *Angew. Chem.* **2015**, *127* (5), 1590−1593.
(28) Jiménez, A. J.; Grimm, B.; Gunderson, V. L.; Vagnini, M. T.; Krick Calderon, S.; Rodríguez-Morgade, M. S.; Wasielewski, M. R.; Guldi, D. M.; Torres, T. Synthesis, Characterization, and Photoinduced Energy and Electron Transfer in a Supramolecular Tetrakis(Ruthenium(II) Phthalocyanine) Perylenediimide Pentad. *Chem. - A Eur. J.* **2011**, *17*, 5024−5032.
(29) Mari, C.; Huang, H.; Rubbiani, R.; Schulze, M.; Würthner, F.; Chao, H.; Gasser, G. Evaluation of Perylene Bisimide-Based RuII and IrIII Complexes as Photosensitizers for Photodynamic Therapy. *Eur. J. Inorg. Chem.* **2017**, *2017*, 1745−1752.
(30) Maia, P. J. S.; de Aguiar, I.; dos Santos Velloso, M.; Zhang, D.; dos Santos, E. R.; de Oliveira, J. R.; Junqueira, J. C.; Selke, M.; Carlos, R. M. Singlet Oxygen Production by a Polypyridine Ruthenium (II) Complex with a Perylene Monoimide Derivative: A Strategy for

https://doi.org/10.1021/acs.inorgchem.3c04569
Inorg. Chem. XXXX, XXX, XXX−XXX

Photodynamic Inactivation of Candida Albicans. *J. Photochem. Photobiol. A Chem.* **2018**, *353*, 536−545.
(31) García-Calvo, J.; Robson, J. A.; Torroba, T.; Wilton-Ely, J. D. E. T. Synthesis and Application of Ruthenium(II) Alkenyl Complexes with Perylene Fluorophores for the Detection of Toxic Vapours and Gases. *Chem. - A Eur. J.* **2019**, *25*, 14214−14222.
(32) Prodi, A.; Chiorboli, C.; Scandola, F.; Iengo, E.; Alessio, E.; Dobrawa, R.; Würthner, F. Wavelength-Dependent Electron and Energy Transfer Pathways in a Side-to-Face Ruthenium Porphyrin/Perylene Bisimide Assembly. *J. Am. Chem. Soc.* **2005**, *127* (5), 1454−1462.
(33) Valore, A.; Balordi, M.; Colombo, A.; Dragonetti, C.; Righetto, S.; Roberto, D.; Ugo, R.; Benincori, T.; Rampinini, G.; Sannicolò, F.; Demartin, F. Novel Ruthenium(Ii) Complexes with Substituted 1,10-Phenanthroline or 4,5-Diazafluorene Linked to a Fullerene as Highly Active Second Order NLO Chromophores. *Dalt. Trans.* **2010**, *39* (42), 10314.
(34) García-Calvo, J.; Torroba, T.; Brañas-Fresnillo, V.; Perdomo, G.; Cózar-Castellano, I.; Li, Y.; Legrand, Y.; Barboiu, M. Manipulation of Transmembrane Transport by Synthetic K + Ionophore Depsipeptides and Its Implications in Glucose-Stimulated Insulin Secretion in B-Cells. *Chem. − Eur. J.* **2019**, *25* (39), 9287−9294.
(35) Frisch, M. J.; Trucks, G. W.; Schlegel, H. B.; Scuseria, G. E.; Robb, M. A.; Cheeseman, J. R.; Scalmani, G.; Barone, V.; Petersson, G. A.; Nakatsuji, H. *Gaussian, 16 Version*; Gaussian Inc.: Wallingford, CT, USA. 2016.
(36) Tomasi, J.; Mennucci, B.; Cammi, R. Quantum Mechanical Continuum Solvation Models. *Chem. Rev.* **2005**, *105* (8), 2999−3094.
(37) Azzaroli, N.; Lapini, A.; Di Donato, M.; Dei, A.; Righini, R. Valence Tautomerism in Co−Dioxolene Complexes: Static and Time-Resolved Infrared Spectroscopy Study. *J. Phys. Chem. B* **2013**, *117* (49), 15492−15502.
(38) Snellenburg, J. J.; Laptenok, S. P.; Seger, R.; Mullen, K. M.; van Stokkum, I. H. M. Glotaran: A Java -Based Graphical User Interface for the R Package TIMP. *J. Stat. Softw.* **2012**, *49* (3), 1−22.
(39) Mede, T.; Jäger, M.; Schubert, U. S. Chemistry-on-the-Complex": Functional Ru II Polypyridyl-Type Sensitizers as Divergent Building Blocks. *Chem. Soc. Rev.* **2018**, *47* (20), 7577−7627.
(40) Hadda, T. B.; Zidane, I.; Moya, S. A.; Bozec, L. H. Soluble ruthenium carbonyl complexes containing new sterically hindered bipyridine ligands. *Polyhedron* **1996**, *15* (9), 1571−1573.
(41) Kang, L.; Wang, B.; Thetford, A.; Wu, K.; Danaie, M.; He, Q.; Gibson, E. K.; Sun, L. D.; Asakura, H.; Catlow, C. R. A.; Wang, F. R. Design, Identification, and Evolution of a Surface Ruthenium(II/III) Single Site for CO Activation. *Angew. Chem., Int. Ed. Engl.* **2021**, *60* (3), 1212−1219.
(42) Rousset, E.; Mongin, O.; Moreau, J.; Lawson-Daku, L. M.; Beley, M.; Gros, P. C.; Chevreux, S.; Blanchard-Desce, M.; Lemercier, G. Molecular Engineering for Optical Properties of 5-Substituted-1,10-Phenanthroline-Based Ru(II) Complexes. *Dalt. Trans.* **2021**, *50* (29), 10119−10132.
(43) Conti, L.; Bencini, A.; Ferrante, C.; Gellini, C.; Paoli, P.; Parri, M.; Pietraperzia, G.; Valtancoli, B.; Giorgi, C. Highly Charged Ruthenium(II) Polypyridyl Complexes as Effective Photosensitizer in Photodynamic Therapy. *Chem. − Eur. J.* **2019**, *25* (45), 10606−10615.
(44) van Stokkum, I. H. M.; Larsen, D. S.; van Grondelle, R. Global and Target Analysis of Time-Resolved Spectra. *Biochim. Biophys. Acta - Bioenerg.* **2004**, *1657* (2−3), 82−104.
(45) Sun, Y.; Liu, Y.; Turro, C. Ultrafast Dynamics of the Low-Lying ^{3}MLCT States of $[Ru(Bpy)_2(Dppp_2)]^{2+}$. *J. Am. Chem. Soc.* **2010**, *132* (16), 5594−5595.
(46) Liu, T.; Han, W.-G.; Himo, F.; Ullmann, G. M.; Bashford, D.; Toutchkine, A.; Hahn, K. M.; Noodleman, L. Density Functional Vertical Self-Consistent Reaction Field Theory for Solvatochromism Studies of Solvent-Sensitive *Dyes. J. Phys. Chem. A* **2004**, *108* (16), 3545−3555.
(47) Boixel, J.; Blart, E.; Pellegrin, Y.; Odobel, F.; Perin, N.; Chiorboli, C.; Fracasso, S.; Ravaglia, M.; Scandola, F. Hole-Transfer Dyads and Triads Based on Perylene Monoimide, Quaterthiophene, and Extended Tetrathiafulvalene. *Chem. − Eur. J.* **2010**, *16* (30), 9140−9153.
(48) Sell, A. C.; Wetzel, J. C.; Schmitz, M.; Maijenburg, A. W.; Woltersdorf, G.; Naumann, R.; Kerzig, C. Water-soluble ruthenium complex-pyrene dyads with extended triplet lifetimes for efficient energy transfer applications. *Dalton Trans.* **2022**, *51* (28), 10799−10808.
(49) Howarth, A. J.; Majewski, M. B.; Wolf, M. O. Photophysical properties and applications of coordination complexes incorporating pyrene. *Coord. Chem. Rev.* **2015**, *282*−*283*, 139−149.
(50) Li, F.; Qian, C.; Lu, J.; Ma, Y.; Zhang, K. Y.; Liu, S.; Zhao, Q. Color-Tunable Dual Persistent Emission Via a Triplet Exciton Reservoir for Temperature Sensing and Anti-Counterfeiting. *Adv. Opt. Mater.* **2022**, *10*, No. 2101773.

https://doi.org/10.1021/acs.inorgchem.3c04569
Inorg. Chem. XXXX, XXX, XXX−XXX